Electronic Supplementary Material (ESI) for Nanoscale.

Supporting Information

Tuning the conductance of a molecular wire by the interplay of donor and acceptor units

Dmitry Skidin[1,2], Tim Erdmann[2,3], Seddigheh Nikipar[1], Frank Eisenhut[1,2], Justus Krüger[1,2], Florian Günther[2,4], Sibylle Gemming[2,4,6], Anton Kiriy[2,3], Brigitte Voit[2,3], Dmitry A. Ryndyk[5], Christian Joachim[7], Francesca Moresco[1,2], and Gianaurelio Cuniberti[1,2]*

[1]Institute for Materials Science, Max Bergmann Center of Biomaterials, TU Dresden, 01062 Dresden, Germany

[2]Center for Advancing Electronics Dresden, TU Dresden, 01062 Dresden, Germany

[3]Leibniz-Institut für Polymerforschung Dresden e.V., 01069 Dresden, Germany

[4]Institute of Ion Beam Physics and Materials Research, Helmholtz-Zentrum Dresden-Rossendorf, Bautzner Landstraße 400, 01328 Dresden, Germany

[5]Bremen Center for Computational Materials Science, Department of Physics, Universität Bremen, 28359 Bremen, Germany

[6]Institute of Physics, TU Chemnitz, 09107 Chemnitz, Germany

[7]GNS & MANA Satellite, CEMES, CNRS, 29 rue J. Marvig, 31055 Toulouse Cedex, France

Contents

Chemical synthesis

Synthesis of the precursors

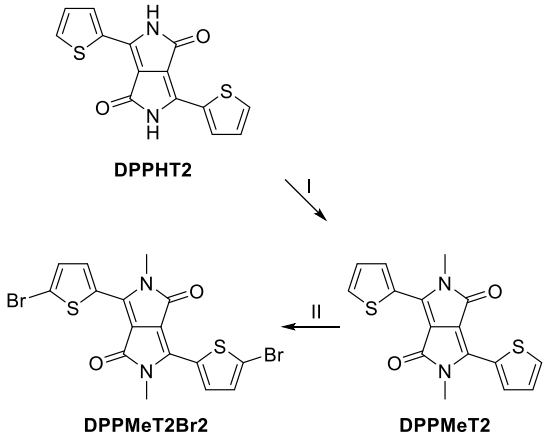

Scheme 1. Synthetic route to DPPMeT2Br2: (I) 18-crown-6, K_2CO_3, MeI, DMF, 120 °C, 16 h, 81%. (II) Pyridine, Br_2, $CHCl_3$, 70 °C, 2 h, 13 %.

The starting DPP-based monomer for performing on-surface polymerization, 3,6-bis(5-bromothiophen-2-yl)-2,5-dimethylpyrrolo[3,4-*c*]pyrrole-1,4(2*H*,5*H*)-dione (DPPMeT2Br2), was obtained in two steps from 3,6-di(thiophen-2-yl)pyrrolo[3,4-*c*]pyrrole-1,4(2*H*,5*H*)-dione (DPPHT2) synthesized according to the literature procedure (Scheme 1).[1] The alkylation of DPPHT2 by using methyl iodide afforded DPPMeT2 in high yields of about 81 %. In comparison to common DPP derivatives equipped with long (branched) alkyl side chains, DPPMeT2 possesses poor solubility in organic solvents and a reduced electron density of the aromatic system due to the weaker +*I* effect of the methyl groups. Consequently, common electrophilic aromatic substitution reagents such as *N*-bromosuccinimide, or solutions of bromine in chloroform, dimethylformamide or acetic acid, failed to convert DPPMeT2 into DPPMeT2Br2, or provided low conversions of the starting material. However we found that the usage of the bromine-pyridine mixture as the bromination agent (which gives *N*-bromopyridinium bromide – the source of a strongly electrophilic bromine cation), lead a smooth and high-yield debromination of the starting material.[2-3]

Instrumentation

Proton (500.13 MHz) and Carbon (125.75 MHz) *nuclear magnetic resonance* (*NMR*) spectra were recorded using a Bruker DRX 500 spectrometer and $CDCl_3$ as solvent. The NMR spectra were referenced to the residual non-deuterated solvent signal (^{1}H NMR: 7.26 ppm and ^{13}C NMR: 77.16 ppm).

Thermogravimetric analysis (TGA) was performed using a TA Instruments Q5000 with a nitrogen gas flow and a heating rate of 10 K/min.

Materials

3,6-Di(thiophen-2-yl)pyrrolo[3,4-*c*]pyrrole-1,4(2*H*,5*H*)-dione (DPPHT2) was synthesized according to published procedures.[1] All other chemicals and solvents were purchased from Sigma Aldrich or Acros Organics and used as received.

Syntheses

2,5-Dimethyl-3,6-di(thiophen-2-yl)pyrrolo[3,4-c]pyrrole-1,4(2H,5H)-dione (DPPMeT2)

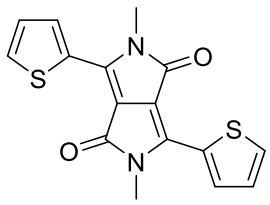

Under nitrogen atmosphere, 2.05 g (6.83 mmol, 1.0 eq.) DPPHT2 were dissolved in 50 ml anhydrous DMF and 0.09 g (0.34 mmol, 0.05 eq.) 18-crown-6 and 3.30 g (23.87 mmol, 3.5 eq.) anhydrous potassium carbonate were added to the solution. The mixture was stirred at 120 °C for 1 h before 4.3 ml (68.25 mmol, 10.0 eq.) methyl iodide were added dropwise over 1 h. After stirring at 120 °C for 16 h, the cooled reaction mixture was concentrated under reduced pressure, diluted with chloroform, washed with water and brine, dried over $MgSO_4$ and evaporated to dryness. The raw product was purified by column chromatography using diethyl ether/chloroform (volume ratio: 100/0 to 0/100). The target compound was obtained as a dark purple solid (1.82 g, 81 %).

^{1}H NMR ($CDCl_3$, 500 MHz) δ [ppm] = 8.89 (dd, 2 H, $^3J_{2/3}$ = 3.9 Hz, $^4J_{1/3}$ = 1.3 Hz), 7.65 (dd, 2 H, $^3J_{1/2}$ = 4.9 Hz, $^4J_{1/3}$ = 1.3 Hz), 7.28 (dd, 2 H, $^3J_{1/2}$ = 4.9 Hz, $^3J_{2/3}$ = 3.9 Hz), 3.62 (s, 6 H). ^{13}C NMR ($CDCl_3$, 125 MHz) δ [ppm] = 161.27 (C_q), 140.51 (C_q), 135.13 (CH), 131.07 (CH), 130.54 (C_q), 128.92 (CH), 107.75 (C_q), 29.37 (CH_3). MALDI-TOF-MS: $[M]^+$ = 328.0 (th. $[M]^+$: 328.03).

3,6-Bis(5-bromothiophen-2-yl)-2,5-dimethylpyrrolo[3,4-*c*]pyrrole-1,4(2*H*,5*H*)-dione (DPPMeT2Br2)

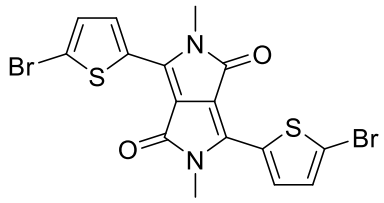

To a mixture of 0.36 g (1.11 mmol, 1.0 eq.) DPPMeT2 and 6.4 ml chloroform were added 0.34 ml (4.10 mmol, 3.7 eq.) pyridine and 0.23 ml (4.44 mmol, 4 eq.) bromine dropwise over a period of 10 min. After stirring at 70 °C for 2 h complete conversion of the starting material was confirmed by TLC and saturated, aqueous solution of $Na_2S_2O_3$ was added. The mixture was poured into methanol and the precipitates were collected, dissolved in acetone/chloroform (volume ratio: 10/90) and passed through a silica gel plug. Finally, the product was further purified by sublimation (200 °C, ≈ 10^{-2} mbar, 72 h) yielding a purple solid (0.07 g, 13 %).
^{1}H NMR ($CDCl_3$, 500 MHz) δ [ppm] = 8.51 (d, 2 H, $^3J_{2/3}$ = 4.2 Hz), 7.28 (d, 2 H, $^3J_{2/3}$ = 4.2 Hz), 3.56 (s, 6 H). ^{13}C NMR ($CDCl_3$, 125 MHz) Very poor solubility, but indications for signals at δ [ppm] = 138.72, 134.37, 131.35, 131.10, 119.27, 117.66, 106.50, 28.65. MALDI-TOF-MS: $[M]^+$ = 483.8 (th. $[M]^+$: 483.86).

Thermogravimetric analysis

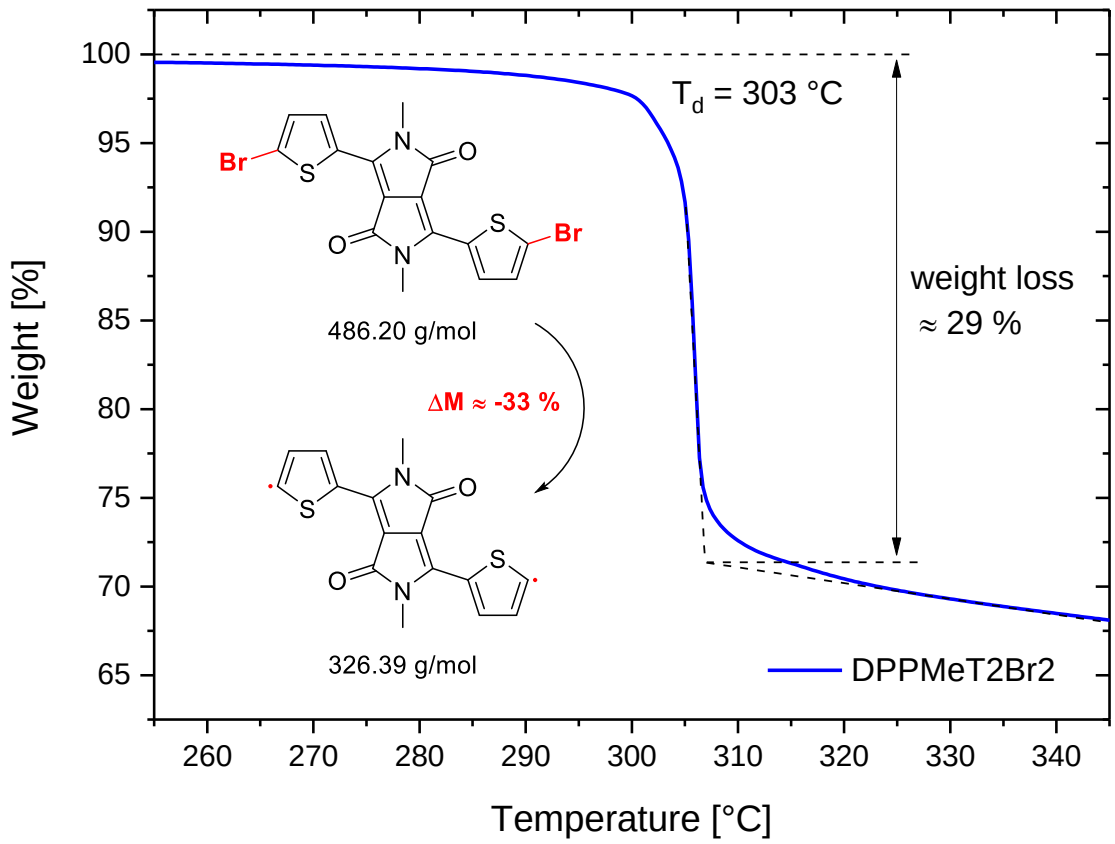

Figure S1. TGA curve of DPPMeT2Br2 and the comparison of theoretical weight loss by debromination with the experimentally observed weight loss. Decomposition temperature T_d was determined at 5 % weight loss.

Additional STM data

Intermediate phase after the first annealing step

Overview STM images

After the annealing at 473 K, the sample is covered with the networks, which grow mostly near the step edges. As can be seen in Figure S2, structures of much smaller apparent height are also largely present (outlined in the black circles). These are the wires and clusters of atomic Br, detached from the monomers after annealing. Red circles outline the structures, which differ in appearance form the networks and are presumably covalently bonded molecular wires fragments.

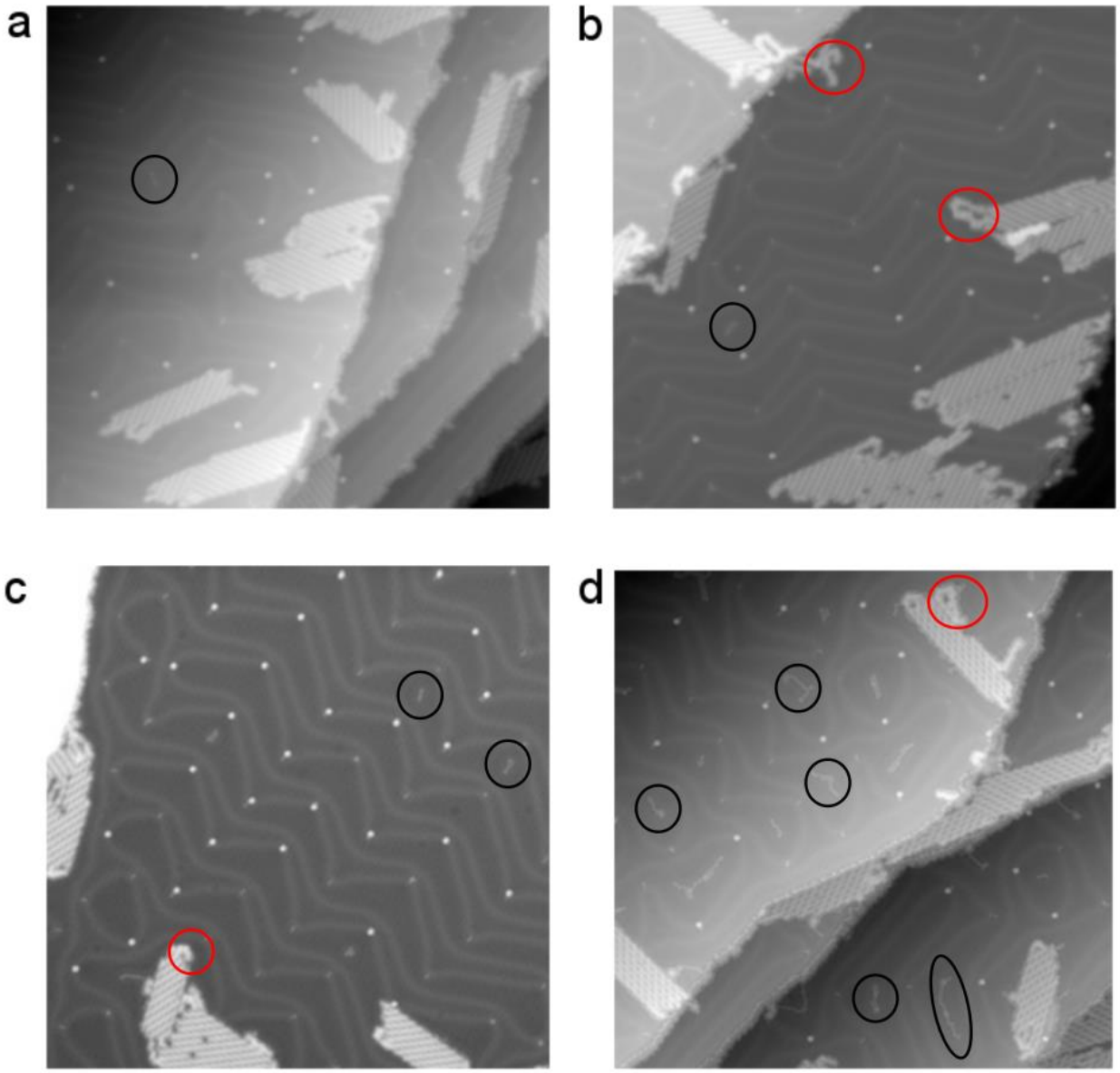

Figure S2. Overview STM images after annealing the sample at 473 K show the tendency of the molecular networks to grow from the step edges. Black circles outline atomic Br, which forms clusters and wires. Red circles mark positions, where covalent molecular wires are extending from the networks or the step edges. All images: U = 0.5 V, I = 20 pA, 80 nm x 80 nm.

dI/dV spectroscopy of the intermediate phase

We performed STS measurements on different positions of the networks after annealing (Figure S3). The spectra taken in the connection area between the monomers show an increased signal at negative bias range exceeding even the signal obtained on the terrace of Au(111) surface. This is the feature known as surface state localization and characteristic to the adatoms on the metal surfaces.[4-5]

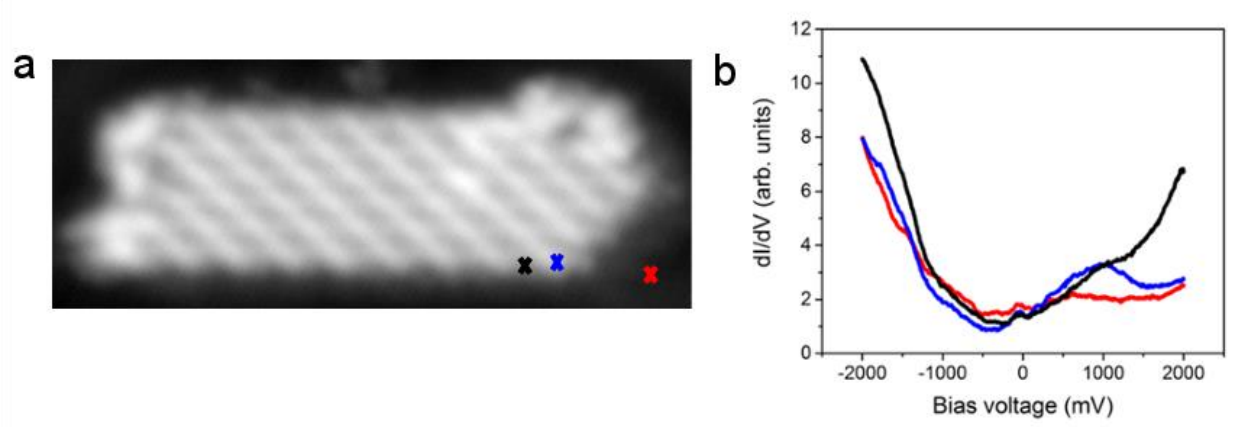

Figure S3. dI/dV spectroscopy on the metal-coordinated network confirms participation of Au adatoms in the bonding of the network. (a) STM image of a small network formed after annealing at 473 K: U = 0.5 V, I = 50 pA, 20 nm x 7.8 nm. (b) dI/dV spectra measured at the positions marked by the crosses of respective colors.

Reconstruction lifting after deposition of the molecules and annealing

To confirm the influence of the molecules adsorption on the Au(111) reconstruction, we compared the distance between the soliton lines for the three cases: clean surface, after deposition of the molecules and further after annealing (Figure S4 and Table S1). For a clean Au(111) surface, we determined the value 6.13±0.27 nm, while after the distortion caused by the deposition of the molecules and subsequent annealing, it is 7.83±0.61 nm. The reconstruction lifting, however, occurs also already after the deposition of the molecules as in this case the distance between the soliton lines is 7.17±0.61 nm. Further annealing promotes debromination of the precursor molecules as well as facilitates diffusion of both molecules and gold adatoms.

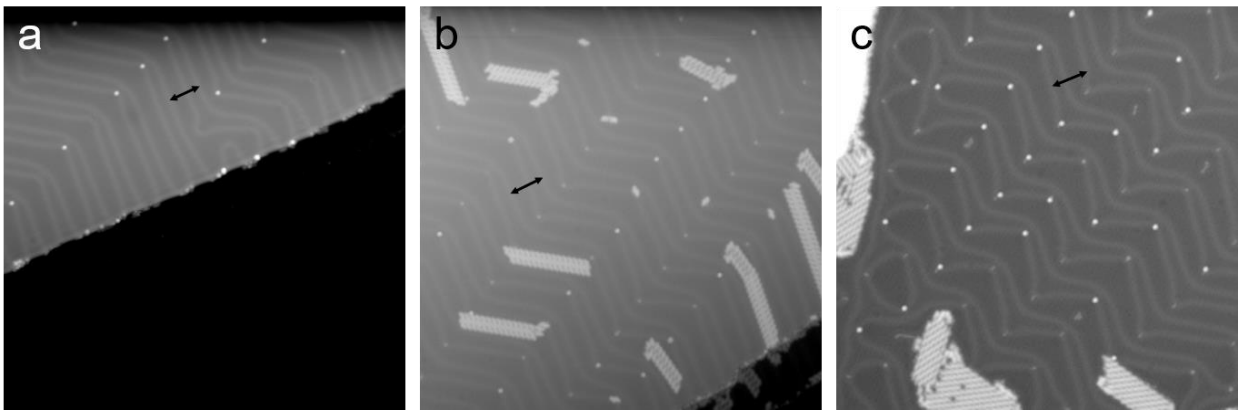

Figure S4. Overview STM images of Au(111) reconstruction at different stages of the sample preparation. (a) Clean surface free of any adsorbates (U = 0.5 V, I = 50 pA). The lower terrace is darkened to increase the contrast of the upper one. (b) Surface after the deposition of the molecules at room temperature (U = 0.5 V, I = 24 pA). (c) Surface after annealing the sample at 473 K (U = 0.5 V, I = 29 pA). The black arrows demonstrate the distance between the soliton lines, which was used as a measure of reconstruction distortion. All images: 80 nm x 80 nm.

Table S1. Soliton distances for the different stages of the sample preparation.

	Distance, nm	Stdev, nm
Clean Au(111)	6.13	0.27
Deposition	7.17	0.39
Annealing 200 ˚C	7.83	0.61

Thus, many Au adatoms are released at this stage – the consequence of the molecular adsorption amplified by the surface annealing. The effect of reconstruction lifting has been previously observed for deposition of thiolates,[6-9] pyridine-functionalized porphyrins[10] and other molecules containing electronegative atoms[11-15]. Interestingly, most of these molecular systems contain sulfur or oxygen groups, which have a high affinity to gold. In the studied DPP molecule, both sulfur and oxygen atoms are present in the donor thiophene and acceptor diketopyrrolopyrrole, respectively.

Additional overview STM images of the final molecular wires phase

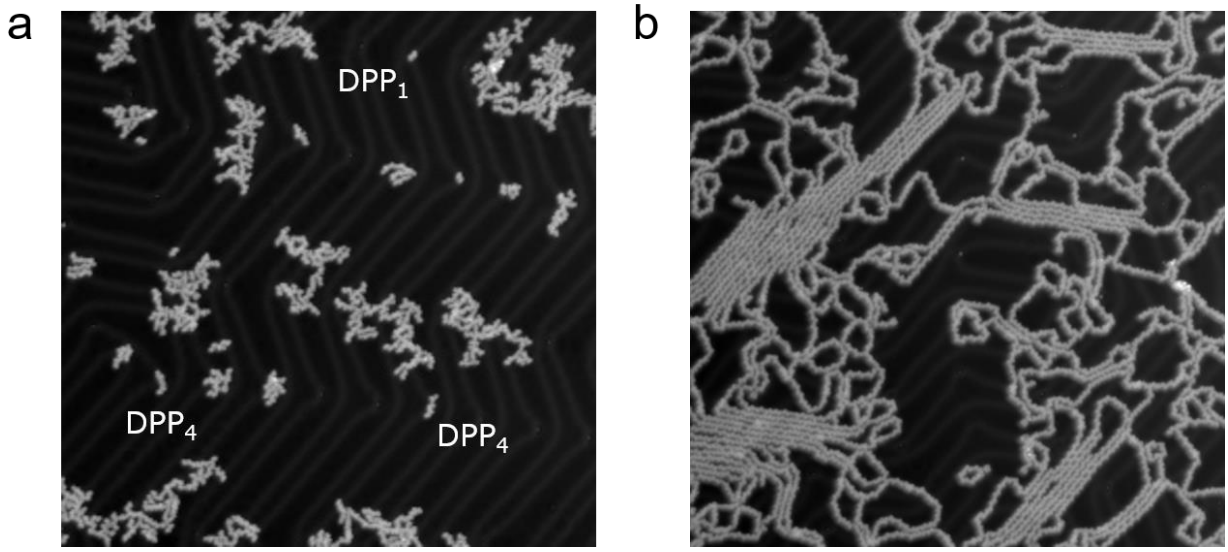

Figure S5. Overview STM images of molecular wires formed after annealing the surface at 260 ˚C. Low surface coverage leads to the short several-monomer wires (a), where DPP_1 corresponds to a single debrominated molecule and DPP_4 to the wire consisting of four repeat units. The areas with a high coverage promote growth of long spaghetti-like molecular wires. Both images: U = 0.5 V, I = 50 pA, 80 nm x 80 nm.

Determination of the monomers orientations in the molecular wires

As it might be of a big importance to determine the preferable orientations of the monomers in the complex polymer structures, we have developed a way to evaluate it from STM images. By measuring the distances between the most protruding parts of the monomers, which correspond to methyl groups, we could obtain a distribution of all possible moieties.

In order to determine the configuration of the units along a polymer wire, we superimposed the STM images with atomic models. For this, DPP-T-T-DPP models were considered (Figure S6), which are able to reproduce all orientations of the polymer backbone. For this model, six different planar configurations can be adopted: tCt, cCt, cCc, tTt, tTc and cTc. In this notation the *cis-trans* conformations between DPP and thiophene is indicated by small "c" or "t" and that between two thiophene rings by capital "C" and "T". For all models, a geometry optimization in gas phase was performed using self-consistent charge density functional based tight binding (SCC-DFTB)[16-17] with the mio-1-1 parameter set.[17-18]

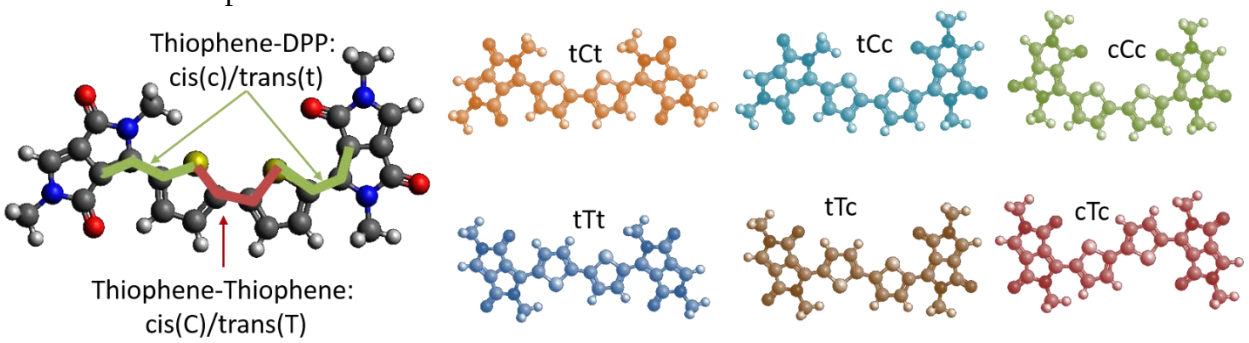

Figure S6. Possible configurations for DPP-T-T- DPP defining the relative positioning of neighboring DPP units.

As demonstrated in Figure S7, the shape of individual molecular wires can be reproduced by this approach. All possible orientations of the DPP-T-T-DPP model were found. In total, we addressed 152 orientations. Among them, about 80% of the configurations between thiophene and DPP were in *trans*.

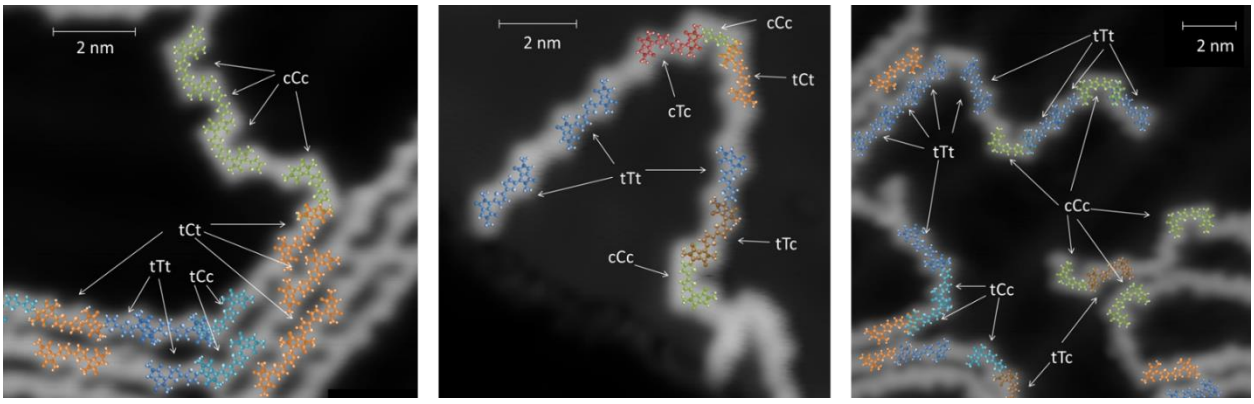

Figure S7. STM images of TDPPT polymer wires superimposed by DPP-T-T-DPP models to determine chain orientation. Imaging parameters: U = 0.1 V, I = 50 pA.

Additional lifting curves

In order to quantitatively evaluate the lifting experiments we had to establish definite selection rules to exclude the lifting curves, which might provide unreliable results. First, only lifting

attempts that resulted in the signal measured at least over 20 Å, were considered for analysis. Excluded were also the curves, in which the oscillations of current did not correspond to the size of a monomer unit. The other factors that were taken into account are the state of the tip before and after the lifting attempt and geometry of a wire on the surface after the lifting.

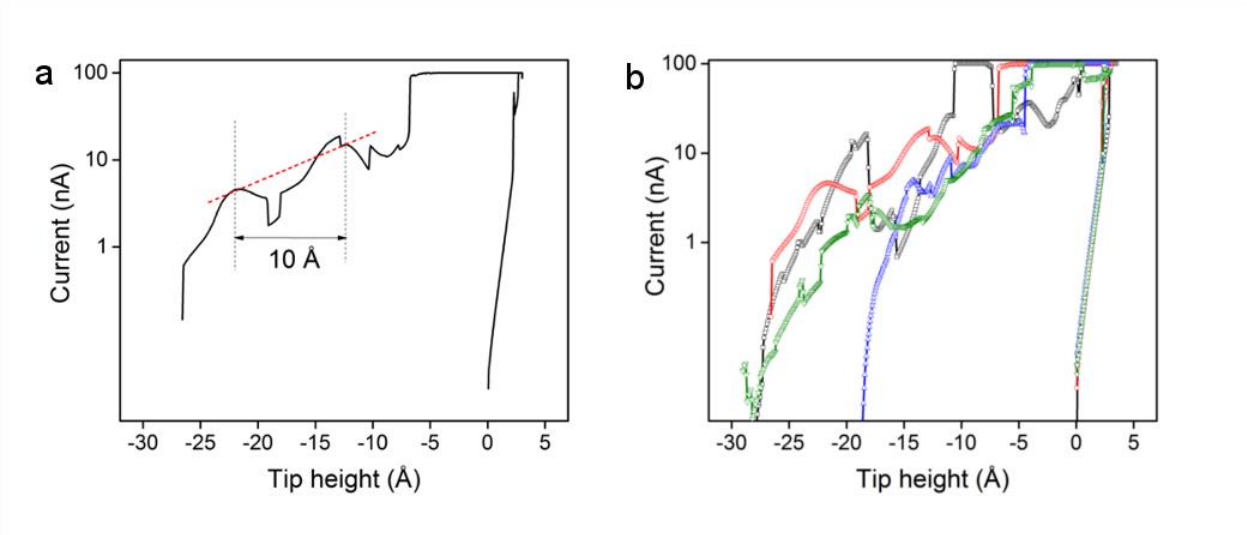

Figure S8. Additional lifting curves. (a) One more lifting example. (b) Cumulative lifting curve, where the attempts with different wires are plotted together.

Complex band structure calculations additional details

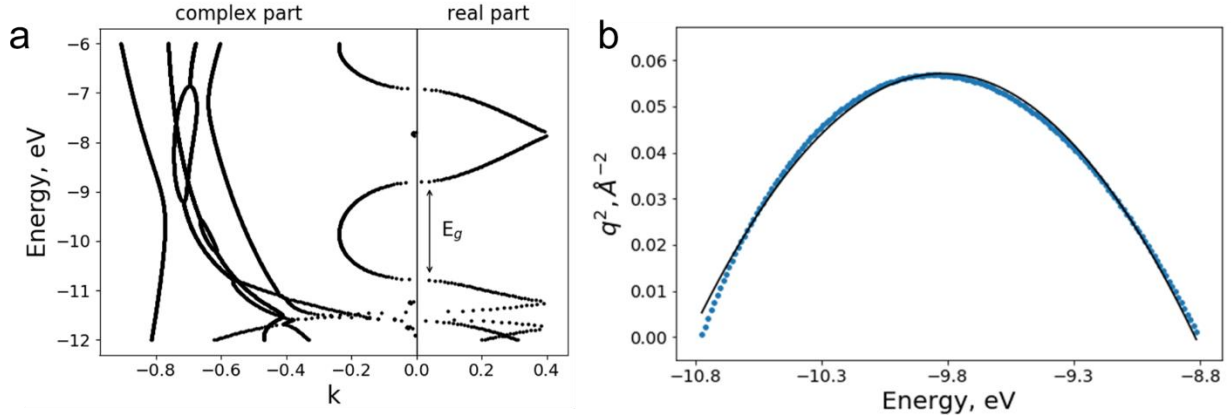

Figure S9. Complex band structure of a polythiophene molecular wire. (a) Full band structure with complex and real parts. (b) Wave vector q^2 as a function of energy in the gap (blue dotted line) is fitted with the quadratic function.

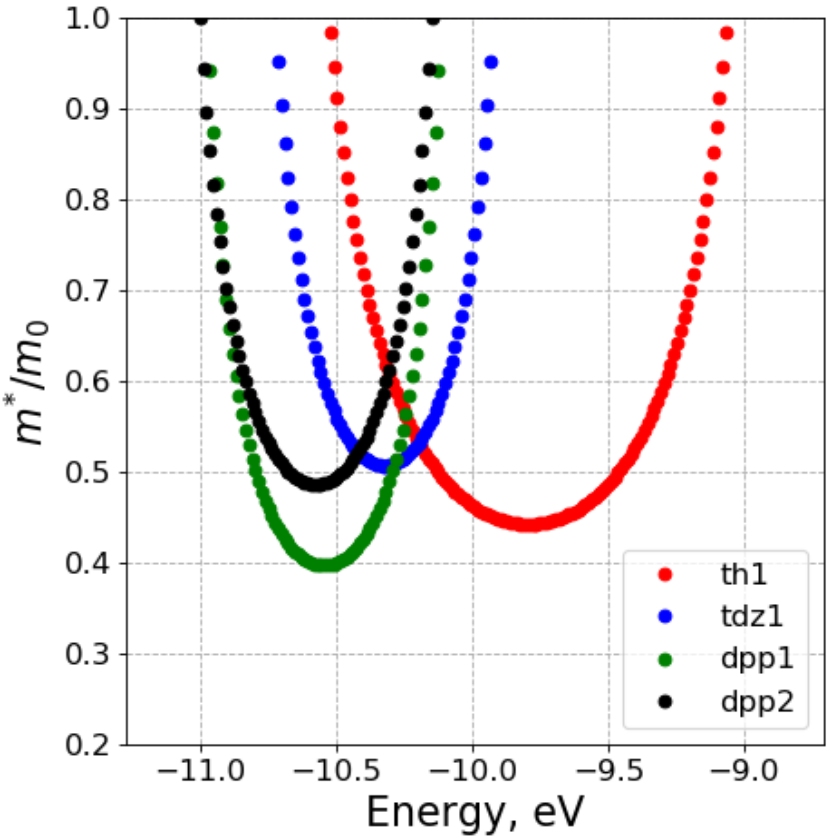

Figure S10. Effective mass of a tunneling electron as a function of energy in the energy gap window. The minimum of each curve corresponds to the Fermi level of the respective molecular wire. Abbreviations according to the Table 1 from the main text.

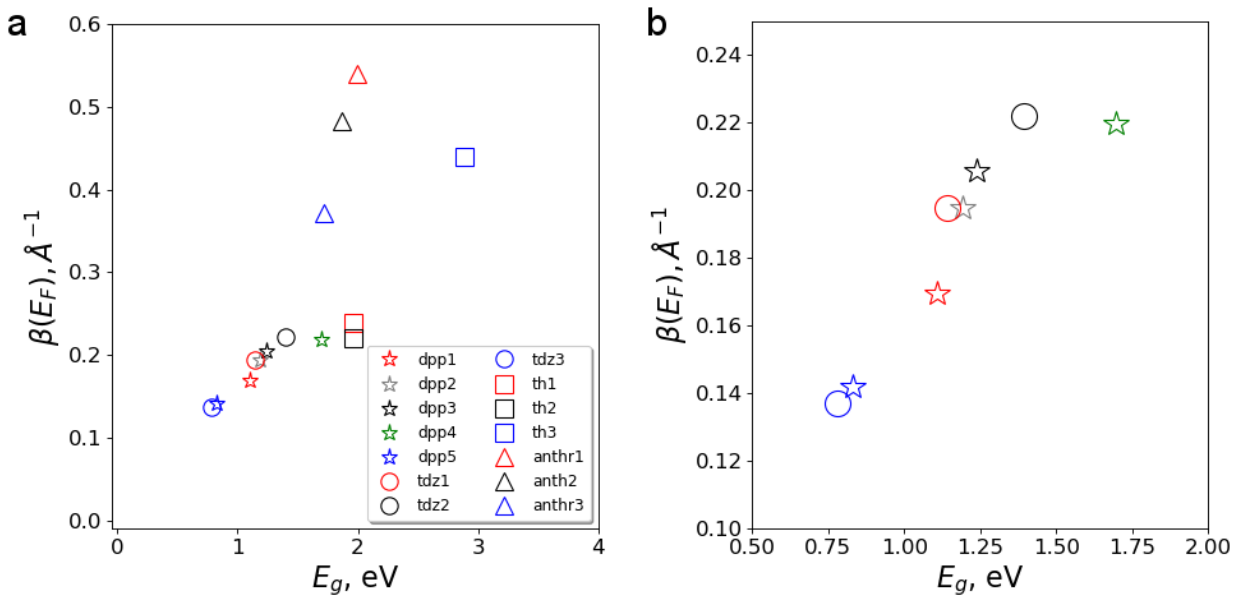

Figure S11. Conductance decay of a number of molecular wires as a function of the energy gap. A zoom-in of a densely packed area of the graph (a) is presented for the case of dpp- and tdz-based wires (b). The markers and abbreviations are as in the main text.

References

1. Karpov, Y.; Erdmann, T.; Raguzin, I.; Al-Hussein, M.; Binner, M.; Lappan, U.; Stamm, M.; Gerasimov, K. L.; Beryozkina, T.; Bakulev, V.; Anokhin, D. V.; Ivanov, D. A.; Günther, F.; Gemming, S.; Seifert, G.; Voit, B.; Di Pietro, R.; Kiriy, A., High Conductivity in Molecularly p-Doped Diketopyrrolopyrrole-Based Polymer: The Impact of a High Dopant Strength and Good Structural Order. *Advanced Materials* **2016,** *28*, 6003-6010.
2. Benin, V.; Yeates, A. T.; Dudis, D., Preparation of halogenated derivatives of thiazolo[5,4-d]thiazole via direct electrophilic aromatic substitution. *J Heterocyclic Chem* **2008,** *45*, 811-819.
3. Acheson, R. M.; Hoult, T. G.; Barnard, K. A., The Bromination of Acridine. *J Chem Soc* **1954**, 4142-4145.
4. Limot, L.; Pehlke, E.; Kroger, J.; Berndt, R., Surface-state localization at adatoms. *Phys Rev Lett* **2005,** *94*.
5. Faraggi, M. N.; Jiang, N.; Gonzalez-Lakunza, N.; Langner, A.; Stepanow, S.; Kern, K.; Arnau, A., Bonding and Charge Transfer in Metal-Organic Coordination Networks on Au(111) with Strong Acceptor Molecules. *J Phys Chem C* **2012,** *116*, 24558-24565.
6. Fitts, W. P.; White, J. M.; Poirier, G. E., Low-coverage decanethiolate structure on Au(111): Substrate effects. *Langmuir* **2002,** *18*, 1561-1566.
7. Maksymovych, P.; Sorescu, D. C.; Yates, J. T., Gold-adatom-mediated bonding in self-assembled short-chain alkanethiolate species on the Au(111) surface. *Phys Rev Lett* **2006,** *97*.
8. Maksymovych, P.; Yates, J. T., Au adatoms in self-assembly of benzenethiol on the Au(111) surface. *Journal of the American Chemical Society* **2008,** *130*, 7518.
9. Voznyy, O.; Dubowski, J. J.; Yates, J. T.; Maksymovych, P., The Role of Gold Adatoms and Stereochemistry in Self-Assembly of Methylthiolate on Au(111). *Journal of the American Chemical Society* **2009,** *131*, 12989-12993.
10. Shi, Z. L.; Lin, N., Porphyrin-Based Two-Dimensional Coordination Kagome Lattice Self-Assembled on a Au(111) Surface. *Journal of the American Chemical Society* **2009,** *131*, 5376.
11. Saywell, A.; Gren, W.; Franc, G.; Gourdon, A.; Bouju, X.; Grill, L., Manipulating the Conformation of Single Organometallic Chains on Au(111). *J Phys Chem C* **2014,** *118*, 1719-1728.
12. Baker, T. A.; Kaxiras, E.; Friend, C. M., Insights from Theory on the Relationship Between Surface Reactivity and Gold Atom Release. *Top Catal* **2010,** *53*, 365-377.
13. Min, B. K.; Deng, X.; Pinnaduwage, D.; Schalek, R.; Friend, C. M., Oxygen-induced restructuring with release of gold atoms from Au(111). *Phys Rev B* **2005,** *72*.
14. Driver, S. M.; Zhang, T. F.; King, D. A., Massively cooperative adsorbate-induced surface restructuring and nanocluster formation. *Angew Chem Int Edit* **2007,** *46*, 700-703.
15. Gao, W. W.; Baker, T. A.; Zhou, L.; Pinnaduwage, D. S.; Kaxiras, E.; Friend, C. M., Chlorine adsorption on Au(111): Chlorine overlayer or surface chloride? *Journal of the American Chemical Society* **2008,** *130*, 3560-3565.
16. Seifert, G., Tight-binding density functional theory: An approximate Kohn-Sham DFT Scheme. *J Phys Chem A* **2007,** *111*, 5609-5613.
17. Elstner, M.; Porezag, D.; Jungnickel, G.; Elsner, J.; Haugk, M.; Frauenheim, T.; Suhai, S.; Seifert, G., Self-consistent-charge density-functional tight-binding method for simulations of complex materials properties. *Phys Rev B* **1998,** *58*, 7260-7268.
18. Niehaus, T. A.; Elstner, M.; Frauenheim, T.; Suhai, S., Application of an approximate density-functional method to sulfur containing compounds. *J Mol Struc-Theochem* **2001,** *541*, 185-194.